Broad Diversity of Near-Infrared Single-Photon Emitters in Silicon

A. Durand,[1] Y. Baron,[1] W. Redjem,[1] T. Herzig,[2] A. Benali,[3] S. Pezzagna,[2] J. Meijer,[2] A. Yu. Kuznetsov,[4] J.-M. Gérard,[5] I. Robert-Philip,[1] M. Abbarchi,[3] V. Jacques,[1] G. Cassabois,[1] and A. Dréau[1,*]

[1] *Laboratoire Charles Coulomb, Université de Montpellier and CNRS, 34095 Montpellier, France*

[2] *Division of Applied Quantum Systems, Felix-Bloch Institute for Solid-State Physics, University Leipzig, Linnéestraße 5, 04103 Leipzig, Germany*

[3] *CNRS, Aix-Marseille Université, Centrale Marseille, IM2NP, UMR 7334, Campus de St. Jérôme, 13397 Marseille, France*

[4] *Department of Physics, University of Oslo, NO-0316 Oslo, Norway*

[5] *Department of Physics, IRIG-PHELIQS, Univ. Grenoble Alpes and CEA, F-38000 Grenoble, France*

(Received 31 August 2020; accepted 21 January 2021; published 22 February 2021)

We report the detection of individual emitters in silicon belonging to seven different families of optically active point defects. These fluorescent centers are created by carbon implantation of a commercial silicon-on-insulator wafer usually employed for integrated photonics. Single photon emission is demonstrated over the 1.1–1.55 μm range, spanning the O and C telecom bands. We analyze their photoluminescence spectra, dipolar emissions, and optical relaxation dynamics at 10 K. For a specific family, we show a constant emission intensity at saturation from 10 K to temperatures well above the 77 K liquid nitrogen temperature. Given the advanced control over nanofabrication and integration in silicon, these individual artificial atoms are promising systems to investigate for Si-based quantum technologies.

DOI: 10.1103/PhysRevLett.126.083602

The boom of silicon in semiconductor technologies was closely tied to the ability to control its density of lattice defects [1]. After being regarded as detrimental to the crystal quality in the first half of the twentieth century [2], point defects have become an essential tool to tune the electrical properties of this semiconductor, leading to the development of a flourishing silicon industry [1]. At the turn of the twenty-first century, progress in Si fabrication and implantation processes has triggered a radical change by enabling the control of these defects at the single defect level [3]. This paradigm shift has brought silicon into the quantum age, where individual dopants are today used as robust quantum bits to encode and process quantum information [4]. These individual qubits can be efficiently controlled and detected by all electrical means [4] but have the drawback of being weakly coupled to light [5] or emitting in the midinfrared range [6] unsuitable for optical fiber propagation. In order to isolate matter qubits that feature an optical interface enabling the long-distance exchange of quantum information while benefiting from well-advanced silicon integrated photonics [7], one strategy is to investigate defects in silicon that are optically active in the near-infrared telecom bands [8,9].

Point defects emitting light exist in various semiconductors [10–12]. While individual solid-state artificial atoms have been observed in several wide band gap semiconductors such as diamond [13,14], silicon carbide [15,16], or hexagonal boron nitride [17], silicon is lagging behind [12]. The first optical detection of a single optically active defect in silicon has only been reported recently [18–20]. This defect is related to a common complex of silicon called the G center, made of an interstitial silicon atom surrounded by two carbon atoms [21–23]. Besides G centers, we report here that silicon, despite its small band gap, hosts a large variety of emitters that can be optically isolated at single scale. We identify six families of individual fluorescent defects in carbon-implanted silicon that emit single photons in the near-infrared range covering the O and C telecom bands. We investigate their photoluminescence spectra, dipolar emissions, and radiative recombination dynamics through lifetime measurements. To conclude, we demonstrate that G centers have a constant emission intensity at saturation from 10 K to well above liquid nitrogen temperatures.

The investigated sample comes from a commercial silicon-on-insulator (SOI) wafer (Soitec). The top 220 nm thick silicon layer (initial residual doping below 1×10^{15} cm^{-3}) was implanted with 36 keV carbon ions at a fluence of 5×10^{13} cm^{-2}. To heal the lattice from damages generated during this process, the sample underwent a subsequent flash annealing at 1050 °C for 20 seconds. The experimental setup consists of a low-temperature scanning confocal microscope operating with above-band-gap optical excitation at 532 nm. The sample photoluminescence (PL) is collected by a high numerical aperture microscope objective (NA = 0.85) and measured with fiber-coupled single-photon detectors featuring a detection efficiency of 10%. The optical detection window was set to cover the near-infrared range from 1.1 to 1.55 μm. More details about the sample preparation and optical setup can be found in [18].

 © 2021 American Physical Society

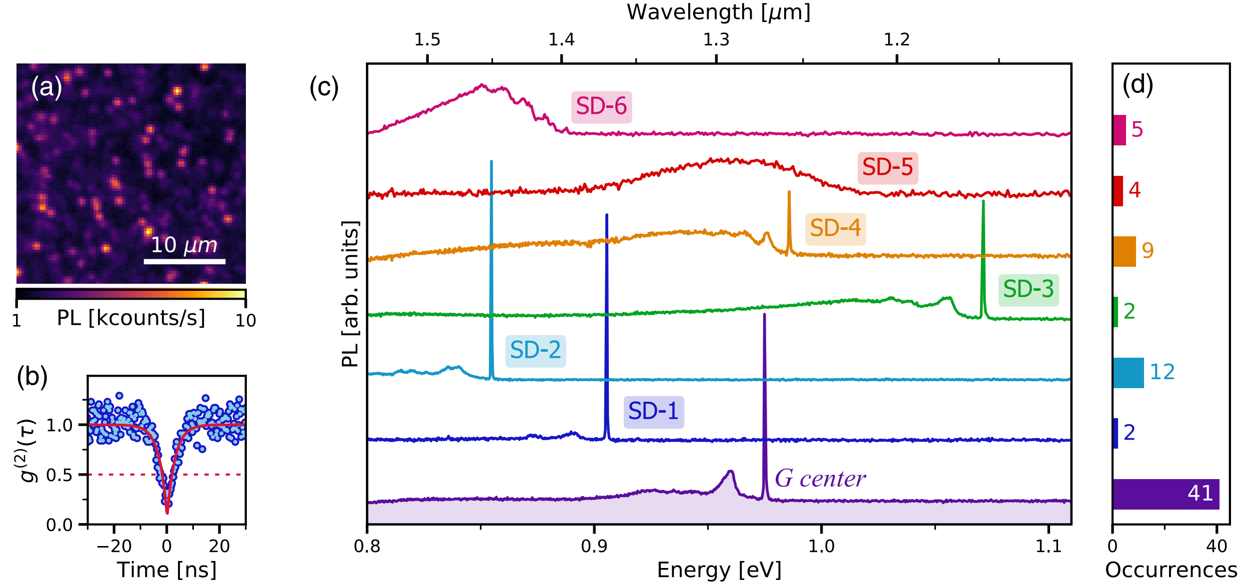

FIG. 1. Isolation of seven families of single defects in silicon. (a) PL raster scan recorded at 10 K under excitation of the carbon-implanted SOI sample with a 532 nm laser at 10 μW. Each isolated bright spot is a single emitter. (b) Second-order autocorrelation function $g^2(\tau)$ measured on a defect belonging to the family SD-1. At zero delay, the curve displays a strong antibunching below the single-emitter threshold: $g^{(2)}(0) < 0.5$. There is no background correction. Data are fitted (solid line) with a two-level model [28]. (c) PL spectra recorded on seven different individual single-photon emitters. The bottom spectrum is associated with the G center in silicon, recently isolated at single scale [18]. The spectra SD-1 to SD-6 correspond to six families of single emitters randomly distributed over the sample. (d) Histogram of the number of defects per family.

A PL image of the sample at 10 K reveals a multitude of fluorescing spots [Fig. 1(a)]. Analyzing their photon emission statistics with a Hanbury-Brown and Twiss setup indicates that all the isolated bright spots appear to be single emitters. Their autocorrelation function $g^{(2)}(\tau)$ presents a clear antibunching that fulfills the single-emitter condition: $g^{(2)}(0) < 0.5$ [24], as displayed in Fig. 1(b) (see the Supplemental Material [25]). By examining the PL spectra of these isolated bright spots [Fig. 1(c)], we observe a broad diversity of emissions between 1.1 and 1.55 μm associated with different fluorescing defects in the C-implanted silicon. Besides individual G centers investigated in a previous study [18], we identify six families of single emitters that we label from SD-1 to SD-6. As their mean zero-phonon line (ZPL) energies match (see Table I), the SD-2 family might be related to interstitial carbon defects C_i associated with an emission line at 856 meV and thought to be a precursor of G centers [21,26]. The other individual single-photon emitters do not appear to be assigned to common luminescent defects in silicon previously identified in the literature through optical spectroscopy on large ensembles [21,27]. Given the small occurrence of those families with respect to the G centers [Fig. 1(d)], one explanation could be that their PL signal detected here at the single defect scale is hidden by the emissions of G centers and possibly other defects in ensemble measurements.

TABLE I. Summary of the optical properties for the different families of single defects. ZPL uncertainties for families G, SD-2, and SD-4 correspond to the standard deviation calculated over the full family set. Statistical data for G centers are taken from Ref. [18]. The histogram of the ZPL energies for families SD-1 to SD-4 and G centers is given in the Supplemental Material [25].

Family	SD-1	SD-2	SD-3	SD-4	SD-5	SD-6	G
Spectrum with ZPL	Yes	Yes	Yes	Yes	No	No	Yes
ZPL energy (meV)	≃905	856 ± 3	≃1071	989 ± 6	⋯	⋯	977 ± 7
ZPL wavelength (nm)	≃1369	1448 ± 5	≃1157	1253 ± 7	⋯	⋯	1269 ± 9
Debye-Waller factor (%)	35	25	3	2	⋯	⋯	15
1st phonon replica energy (meV)	14.5	14.5	14.5	9.5	⋯	⋯	14.5
PL intensity at saturation (kc/s)	13	9	8	14	22	10	16
Resistant to thermal cycles	Yes	Yes	Yes	Yes	No	Yes	Yes
Number of emission dipoles	1	1	1	1	1	1	1
ES lifetime(s) (ns)	14.4 ± 0.4	30.6 ± 0.5	30 ± 1	26 ± 1	4.4 ± 0.7 19 ± 5	6.7 ± 0.8 35 ± 4	36 ± 4

These individual defects in silicon all emit in the near-infrared region. Their PL can even match the O to C telecom bands that cover the range from 1.26 to 1.56 μm. We first observe that the PL spectrum strongly differs from one type of defect to another. While the ZPL dominates over the vibronic spectrum for families SD-1 and SD-2, it becomes less and less intense for families SD-3 and SD-4 and then undetectable for families SD-5 and SD-6 [Fig. 1(c)]. The Debye-Waller factor meters the proportion of photons emitted in the ZPL and provides information about the electron-phonon coupling [29]. As indicated in Table I, the proportion reaches values as high as 35% and 25% for the SD-1 and SD-2 defects, respectively, whereas it is limited to 2–3% for families SD-3 and SD-4. A closer inspection of the phonon sideband reveals that the first phonon replica appears at 9.5 meV (SD-4) or 14.5 meV (SD-1 to SD-3, G center), as depicted in Fig. 2(a) and Table I. We note that the phonon sideband of family SD-6 exhibits a periodicity of 9.5 meV. Since these energies do not correspond to any of the maxima of the silicon-phonon density of states [Fig. 2(a)], the vibronic spectrum likely results from phonons combining localized and Bloch vibrational states [30].

Comparing the ZPL position for the most prevalent families SD-2 and G shows two radically different distributions. The ZPL position randomly spreads over 20 meV around 977 meV for the G centers due to local strain variations [31] [Figs. 2(b), 2(d)]. By contrast, the ZPL of SD-2 defects is always found at three different energies equally split by 3 meV around 856 meV [Figs. 2(c), 2(e)]. Such a behavior suggests that three defect configurations which are less sensitive to local strain fluctuations exist for the SD-2 defects. This could be an appealing property in the prospects of developing indistinguishable single-photon emissions [32]. We note that the average ZPL position for SD-2 centers matches the 856 meV value reported for interstitial carbon defects [26]. Advanced theoretical calculations would be required to explain the observed ZPL distribution.

Besides being near-infrared single-photon emitters, these single defects in silicon share additional interesting PL properties. First, these individual emitters are perfectly photostable, with neither blinking nor bleaching observed while recording their PL signals over time. Furthermore, no center fades away after warming up to room temperature followed by cooling down to 10 K except for the defects of family SD-5, which either disappear or appear in optical scans [25]. In particular, although a prolongated annealing at 300 K has been reported to convert interstitial carbon defects C_i into G centers [26], we have not observed any conversion from SD-2 defects into G centers. Then, like individual G centers in silicon [18], these single-photon emitters show a bright emission under green optical excitation, with PL intensity at saturation on the order of 10–20 kcounts/s (Table I). These PL count rates are high considering the

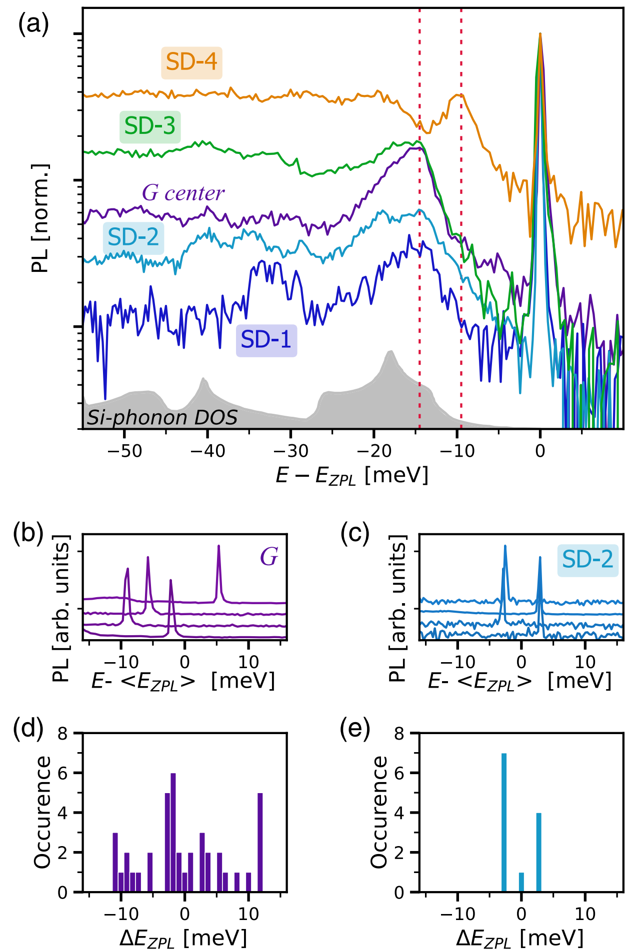

FIG. 2. Spectral properties of individual defects. (a) Comparison of the phonon sideband for the defects with a ZPL. The spectra are normalized to the ZPL maximum and plotted with respect to their ZPL energy E_{ZPL}. The vertical lines show the position of the first phonon replica at 9.5 meV and 14.5 meV. The gray-shaded area indicates the silicon-phonon density of states. (b),(c) Typical PL spectra measured on individual defects for families G and SD-2, respectively. The spectra are plotted with respect to the mean ZPL energy position $\langle E_{\mathrm{ZPL}} \rangle$. (d),(e) Distribution of the ZPL energy shift compared to the middle energy for the same defect families.

poor quantum efficiency of our detectors (only 10%) and that we collect for optimal dipole orientation and position, at best 2% of the emitted photons due to the high refractive index of silicon ($n \sim 3.5$) [18]. Lastly, all defect families emit linearly polarized single photons. As shown in Fig. 3(a) for families SD-1 to SD-4, each of the PL polarization diagrams measured on individual centers shows the characteristic emission of a single dipole [33] (see [25] for families SD-5 and SD-6). We note that the dipole orientation angle can vary from one defect to another inside a given family, but our dataset is insufficient to provide statistically relevant distributions for the dipole angles. Although the interstitial Si atom inside the G centers as well as interstitial carbons are reported to be mobile respectively above 30 K [34] and 77 K [21], we

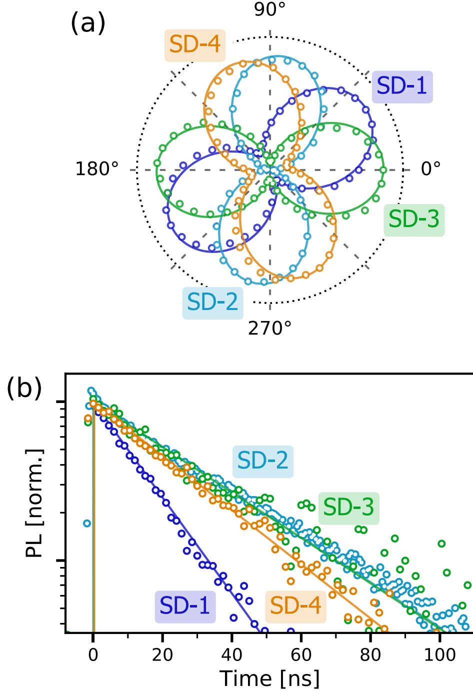

FIG. 3. PL polarization and excited state lifetime measurements. (a) Emission polarization diagram measured on single defects from families SD-1 to SD-4. The PL signal is recorded while rotating a polarizer in the detection path and corrected from background counts. The 0° and 90° directions match the crystal axes [110] and [1$\bar{1}$0]. Solid lines are fits using a $\cos^2(\theta)$ function. (b) Time-resolved PL decay recorded on the same defects under 50 ps pulse excitation at 532 nm. The excited-state lifetime is extracted by fitting the data with a single exponential function (solid line). Data related to SD-5 and SD-6 defects can be found in the Supplemental Material [25].

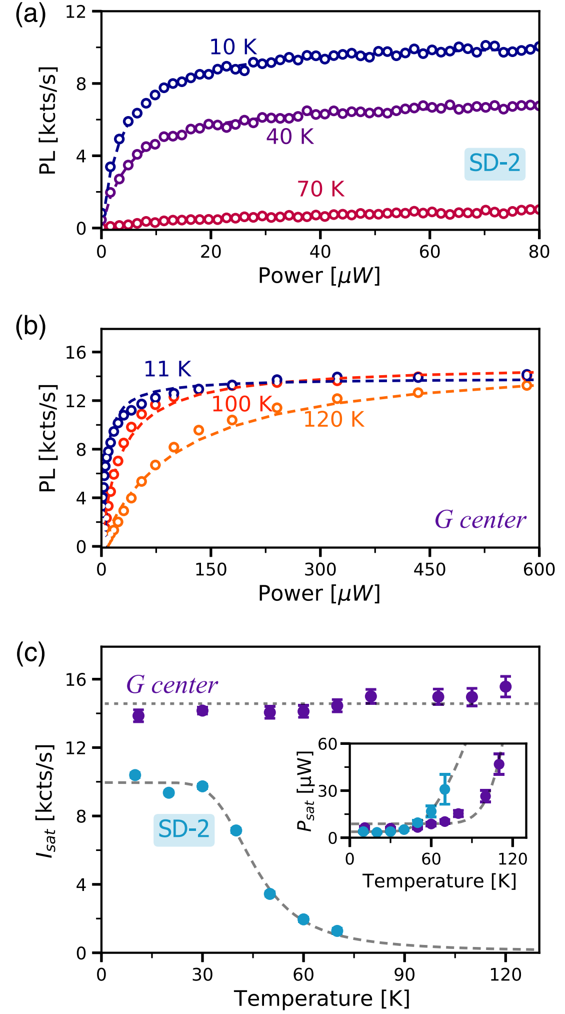

FIG. 4. Evolution of the optical saturation curves with temperature. (a),(b) Background-corrected PL saturation curves measured respectively on a single G defect and a single SD-2 defect for different temperatures. Data is fitted with Eq. (1) to extract the saturation power $P_{\rm sat}$ and intensity at saturation $I_{\rm sat}$. (c) Corresponding evolution of $I_{\rm sat}$ and $P_{\rm sat}$ (inset) with temperature for the SD-2 (blue) and G (purple) defects. The dash lines are data fitting (see main text for $P_{\rm sat}$ data). The $I_{\rm sat}$ data for the SD-2 defect are fairly reproduced by the function $a'/\{1+b'\exp[-E_{a2}/(k_BT)]\}$, where a' and b' are free parameters and $E_{a2} = 24 \pm 3$ meV is the activation energy. The dotted line for the G data is a guide for the eye.

did not observe any change in the emission polarization diagram of the G and SD-2 defects at 130 K and 70 K, respectively, or after successive thermal cycles of the cryostat [25].

To characterize the relaxation dynamics of the individual single-photon emitters, we performed time-resolved PL measurements under 532 nm pulse excitation. The photon histograms recorded on single defects belonging to families SD-1 to SD-4 are shown in Fig. 3(b). For those four families, we observe a monoexponential decay providing a single excited-state (ES) lifetime ranging between 14 to 30 ns (Table I). In contrast, families SD-5 and SD-6 feature a biexponential decay with a short lifetime at roughly 5 ns and long ones around 19 ns and 35 ns, respectively (see Table I and the Supplemental Material). All these values are orders of magnitude shorter than the ones measured on emitter ensembles in silicon, e.g., erbium dopants [9] or T centers [8]. Consequently, these defects are already advantageous to develop bright Si-based single-photon sources even without requiring PL enhancement by Purcell effect [35].

Finally, we analyze the PL saturation curves as a function of temperature. Here we focus on the most frequent families SD-2 and G [Fig. 1(d)]. Figure 4(a) and 4(b) show the PL intensity evolution with optical power P at different temperatures for two single SD-2 and G defects. The data follow the behavior from a two-level system modeled by the standard saturation equation

$$I(P) = I_{\rm sat}\frac{P}{P + P_{\rm sat}}, \qquad (1)$$

with I_{sat} being the maximum PL intensity at saturation and P_{sat} the saturation power. We observe for both defects a rise of P_{sat} with increasing temperature [Fig. 4(c) inset]. This behavior stems from the thermal activation of non-radiative decay channels, as evidenced by the decrease of ES lifetimes at elevated temperatures [22] (see the Supplemental Material [25]). The evolution of P_{sat} with temperature T is fitted with $a + b\exp[-E_{a1}/(k_B T)]$, with a and b as free constants, k_B the Boltzmann constant, and E_{a1} the activation energy that gives the respective values $E_{a1}^{(\mathrm{SD}-2)} = 25 \pm 1$ meV and $E_{a1}^{(\mathrm{G})} = 95 \pm 9$ meV for SD-2 and G defects. The most striking feature is related to the PL intensity at saturation: while I_{sat} drops quickly above 30 K for the family SD-2, it stays constant for G centers well above the 77 K liquid nitrogen temperature (Fig. 4). Since the PL counts mirror the ES population of the emitters, this indicates that the G defects behave as a closed system when the temperature rises, whereas the SD-2 defects are coupled to their environment.

In conclusion, we report the isolation at the single defect scale of seven families of optically active point defects in silicon. These individual emitters provide a wide diversity of bright, linearly polarized single-photon emissions in the near-infrared range, some even matching the O and C telecom bands. We further demonstrate that some single defects exhibit additional appealing properties, such as a small spread of the ZPL energies or a strong PL intensity well above the liquid nitrogen temperature.

This multitude of fluorescent artificial atoms available in silicon could open a new path in exploring Si-based quantum technologies. These single defects could serve as building blocks to develop efficient and deterministic sources of photonic qubits in a material widely used for integrated photonics applications [7,36]. Combining optical and microwave magnetic excitations could enable the investigation of the spin properties attached to these unidentified single-photon emitters in view of isolating individual spin-photon interfaces in silicon operating at telecom wavelengths [8]. The advance nanotechnology based on this semiconductor, combined with the myriad of available defects [21,27], points the way toward thriving quantum applications based on single defects in silicon [10,37].

This work was supported by the French National Research Agency (ANR) through the projects ULYSSES (No. ANR-15-CE24-0027-01), OCTOPUS (No. ANR-18-CE47-0013-01) and QUASSIC (ANR-18-ERC2-0005-01), the German Research Foundation (DFG) through the ULYSSES project (PE 2508/1-1) and the European Union's Horizon 2020 program through the FET-OPEN project NARCISO (No. 828890). The Research Council of Norway is acknowledged for the support to the Norwegian Micro- and Nano-Fabrication Facility, NorFab (Project No. 295864). The authors thank the Nanotecmat platform of the IM2NP institute. A. Durand acknowledges support from the French DGA.

---

[*]Corresponding author.
anais.dreau@umontpellier.fr

[1] *Defects and Impurities in Silicon Materials: An Introduction to Atomic-Level Silicon Engineering*, edited by Y. Yoshida and G. Langouche, Vol. 916 of Lecture Notes in Physics (Springer, Tokyo, 2015).

[2] H. J. Queisser and E. E. Haller, Defects in semiconductors: Some fatal, some vital, Science **281**, 945 (1998).

[3] A. Morello, J. J. Pla, F. A. Zwanenburg, K. W. Chan, K. Y. Tan, H. Huebl, M. Möttönen, C. D. Nugroho, C. Yang, J. A. van Donkelaar, A. D. C. Alves, D. N. Jamieson, C. C. Escott, L. C. L. Hollenberg, R. G. Clark, and A. S. Dzurak, Single-shot readout of an electron spin in silicon, Nature (London) **467**, 687 (2010).

[4] Y. He, S. K. Gorman, D. Keith, L. Kranz, J. G. Keizer, and M. Y. Simmons, A two-qubit gate between phosphorus donor electrons in silicon, Nature (London) **571**, 371 (2019).

[5] M. Steger, K. Saeedi, M. L. W. Thewalt, J. J. L. Morton, H. Riemann, N. V. Abrosimov, P. Becker, and H.-J. Pohl, Quantum information storage for over 180 s using donor spins in a 28Si semiconductor vacuum, Science **336**, 1280 (2012).

[6] K. J. Morse, R. J. S. Abraham, A. DeAbreu, C. Bowness, T. S. Richards, H. Riemann, N. V. Abrosimov, P. Becker, H.-J. Pohl, M. L. W. Thewalt, and S. Simmons, A photonic platform for donor spin qubits in silicon, Sci. Adv. **3**, e1700930 (2017).

[7] J. W. Silverstone, D. Bonneau, J. L. O'Brien, and M. G. Thompson, Silicon quantum photonics, IEEE J. Sel. Top. Quantum Electron. **22**, 390 (2016).

[8] L. Bergeron, C. Chartrand, A. T. K. Kurkjian, K. J. Morse, H. Riemann, N. V. Abrosimov, P. Becker, H.-J. Pohl, M. L. W. Thewalt, and S. Simmons, Silicon-Integrated Telecommunications Photon-Spin Interface, PRX Quantum **1**, 020301 (2020).

[9] L. Weiss, A. Gritsch, B. Merkel, and A. Reiserer, Erbium dopants in silicon nanophotonic waveguides, Optica **8**, 40 (2021).

[10] J. R. Weber, W. F. Koehl, J. B. Varley, A. Janotti, B. B. Buckley, C. G. Van de Walle, and D. D. Awschalom, Quantum computing with defects, Proc. Natl. Acad. Sci. U.S.A. **107**, 8513 (2010).

[11] I. Aharonovich, D. Englund, and M. Toth, Solid-state single-photon emitters, Nat. Photonics **10**, 631 (2016).

[12] G. Zhang, Y. Cheng, J.-P. Chou, and A. Gali, Material platforms for defect qubits and single-photon emitters, Appl. Phys. Rev. **7**, 031308 (2020).

[13] A. Gruber, A. Dräbenstedt, C. Tietz, L. Fleury, J. Wrachtrup, and C. V. Borczyskowski, Scanning confocal optical microscopy and magnetic resonance on single defect centers, Science **276**, 2012 (1997).

[14] C. Bradac, W. Gao, J. Forneris, M. E. Trusheim, and I. Aharonovich, Quantum nanophotonics with group IV defects in diamond, Nat. Commun. **10**, 5625 (2019).

[15] D. J. Christle, A. L. Falk, P. Andrich, P. V. Klimov, J. U. Hassan, N. T. Son, E. Janzén, T. Ohshima, and D. D. Awschalom, Isolated electron spins in silicon carbide with millisecond coherence times, Nat. Mater. **14**, 160 (2015).

[16] M. Widmann, S.-Y. Lee, T. Rendler, N. T. Son, H. Fedder, S. Paik, L.-P. Yang, N. Zhao, S. Yang, I. Booker, A. Denisenko, M. Jamali, S. A. Momenzadeh, I. Gerhardt, T. Ohshima, A. Gali, E. Janzén, and J. Wrachtrup, Coherent control of single spins in silicon carbide at room temperature, Nat. Mater. **14**, 164 (2015).

[17] T. T. Tran, K. Bray, M. J. Ford, M. Toth, and I. Aharonovich, Quantum emission from hexagonal boron nitride monolayers, Nat. Nanotechnol. **11**, 37 (2016).

[18] W. Redjem, A. Durand, T. Herzig, A. Benali, S. Pezzagna, J. Meijer, A. Y. Kuznetsov, H. S. Nguyen, S. Cueff, J.-M. Gérard, I. Robert-Philip, B. Gil, D. Caliste, P. Pochet, M. Abbarchi, V. Jacques, A. Dréau, and G. Cassabois, Single artificial atoms in silicon emitting at telecom wavelengths, Nat. Electron. **3**, 738 (2020).

[19] M. Hollenbach, Y. Berencén, U. Kentsch, M. Helm, and G. V. Astakhov, Engineering telecom single-photon emitters in silicon for scalable quantum photonics, Opt. Express **28**, 26111 (2020).

[20] S. Simmons, A single silicon colour centre resolved, Nat. Electron. **3**, 734 (2020).

[21] G. Davies, The optical properties of luminescence centres in silicon, Phys. Rep. **176**, 83 (1989).

[22] C. Beaufils, W. Redjem, E. Rousseau, V. Jacques, A. Y. Kuznetsov, C. Raynaud, C. Voisin, A. Benali, T. Herzig, S. Pezzagna, J. Meijer, M. Abbarchi, and G. Cassabois, Optical properties of an ensemble of G-centers in silicon, Phys. Rev. B **97**, 035303 (2018).

[23] C. Chartrand, L. Bergeron, K. J. Morse, H. Riemann, N. V. Abrosimov, P. Becker, H.-J. Pohl, S. Simmons, and M. L. W. Thewalt, Highly enriched ^{28}Si reveals remarkable optical linewidths and fine structure for well-known damage centers, Phys. Rev. B **98**, 195201 (2018).

[24] M. D. Eisaman, J. Fan, A. Migdall, and S. V. Polyakov, Invited review article: Single-photon sources and detectors, Rev. Sci. Instrum. **82**, 071101 (2011).

[25] See Supplemental Material at http://link.aps.org/supplemental/10.1103/PhysRevLett.126.083602 for additional experimental data.

[26] K. Thonke, A. Teschner, and R. Sauer, New photoluminescence defect spectra in silicon irradiated at 100 K: Observation of interstitial carbon?, Solid State Commun. **61**, 241 (1987).

[27] P. Pichler, Intrinsic point defects, impurities, and their diffusion in silicon, *Computational Microelectronics* (Springer-Verlag, Wien, 2004).

[28] A. Beveratos, R. Brouri, J.-P. Poizat, and P. Grangier, Bunching and antibunching from single NV color centers in diamond, in *Quantum Communication, Computing, and Measurement 3*, edited by P. Tombesi and O. Hirota, Boston, (Springer, MA, 2002), pp. 261–267.

[29] C. E. Dreyer, A. Alkauskas, J. L. Lyons, A. Janotti, and C. G. Van de Walle, First-principles calculations of point defects for quantum technologies, Annu. Rev. Mater. Res. **48**, 1 (2018).

[30] S. K. Estreicher, D. West, J. Goss, S. Knack, and J. Weber, First-Principles Calculations of Pseudolocal Vibrational Modes: The Case of Cu and Cu Pairs in Si, Phys. Rev. Lett. **90**, 035504 (2003).

[31] V. D. Tkachev and A. V. Mudryi, Piezospectroscopic effect on zero-phonon luminescence lines of silicon, J. Appl. Spectrosc. **29**, 1485 (1978).

[32] A. Sipahigil, K. D. Jahnke, L. J. Rogers, T. Teraji, J. Isoya, A. S. Zibrov, F. Jelezko, and M. D. Lukin, Indistinguishable Photons from Separated Silicon-Vacancy Centers in Diamond, Phys. Rev. Lett. **113**, 113602 (2014).

[33] R. J. Elliott, I. G. Matthew, and E. W. J. Mitchell, The polarization of luminescence in diamond, Philos. Mag. **3**, 360 (1958).

[34] K. P. O'Donnell, K. M. Lee, and G. D. Watkins, Origin of the 0.97 eV luminescence in irradiated silicon, Physica (Amsterdam) **116B+C**, 258 (1983).

[35] E. M. Purcell, H. C. Torrey, and R. V. Pound, Resonance absorption by nuclear magnetic moments in a solid, Phys. Rev. **69**, 37 (1946).

[36] X. Qiang, X. Zhou, J. Wang, C. M. Wilkes, T. Loke, S. O'Gara, L. Kling, G. D. Marshall, R. Santagati, T. C. Ralph, J. B. Wang, J. L. O'Brien, M. G. Thompson, and J. C. F. Matthews, Large-scale silicon quantum photonics implementing arbitrary two-qubit processing, Nat. Photonics **12**, 534 (2018).

[37] P. M. Koenraad and M. E. Flatté, Single dopants in semiconductors, Nat. Mater. **10**, 91 (2011).